

C-Terminal Tyrosine of Ferredoxin–NADP⁺ Reductase in Hydride Transfer Processes with NAD(P)⁺/H[†]

Jesús Tejero,[‡] Inmaculada Pérez-Dorado,[§] Celia Maya,[§] Marta Martínez-Júlvez,[‡] Julia Sanz-Aparicio,[§] Carlos Gómez-Moreno,[‡] Juan A. Hermoso,[§] and Milagros Medina^{*,‡}

Departamento de Bioquímica y Biología Molecular y Celular, Facultad de Ciencias, and Institute of Biocomputation and Physics of Complex Systems (BIFI), Universidad de Zaragoza, E-50009 Zaragoza, Spain, and Grupo de Cristalografía Macromolecular y Biología Estructural, Instituto Química-Física Rocasolano, CSIC, Serrano 119, 28006 Madrid, Spain

Received July 4, 2005; Revised Manuscript Received August 16, 2005

ABSTRACT: Ferredoxin–NADP⁺ reductase (FNR) catalyzes the reduction of NADP⁺ to NADPH in an overall reversible reaction, showing some differences in the mechanisms between cyanobacterial and higher plant FNRs. During hydride transfer it is proposed that the FNR C-terminal Tyr is displaced by the nicotinamide. Thus, this C-terminal Tyr might be involved not only in modulating the flavin redox properties, as already shown, but also in nicotinamide binding and hydride transfer. FNR variants from the cyanobacterium *Anabaena* in which the C-terminal Tyr has been replaced by Trp, Phe, or Ser have been produced. All FNR variants show enhanced NADP⁺ and NAD⁺ binding, especially Tyr303Ser, which correlates with a noticeable improvement of NADH-dependent reactions. Nevertheless, the Tyr303Ser variant shows a decrease in the steady-state k_{cat} value with NADPH. Fast kinetic analysis of the hydride transfer shows that the low efficiency observed for this mutant FNR under steady-state conditions is not due to a lack of catalytic ability but rather to the strong enzyme–coenzyme interaction. Three-dimensional structures for Tyr303Ser and Tyr303Trp variants and its complexes with NADP⁺ show significant differences between plant and cyanobacterial FNRs. Our results suggest that modulation of coenzyme affinity is highly influenced by the strength of the C-terminus–FAD interaction and that subtle changes between plant and cyanobacterial structures are able to modify the energy of that interaction. Additionally, it is shown that the C-terminal Tyr of FNR lowers the affinity for NADP⁺/H to levels compatible with steady-state turnover during the catalytic cycle, but it is not involved in the hydride transfer itself.

Ferredoxin–NADP⁺ reductase (FNR,¹ EC 1.18.1.2) is a FAD-dependent enzyme that catalyzes the electron transfer (ET) from reduced protein electron carriers, ferredoxin or flavodoxin, to NADP⁺ in the last step of the photosynthetic electron transfer chain to produce NADPH (1–4). The reaction is highly specific for NADP⁺/H, the enzyme showing a dramatic decrease in activity when NAD⁺/H is used as coenzyme (5, 6). Three-dimensional structures of FNRs from different sources, as well as of several mutant FNRs and in complex with its substrates, are available (7–15). The structure consists of two distinct domains: an N-terminal FAD binding domain and a C-terminal domain that binds the NADP⁺ coenzyme (Figure 1A). This two-

domain motif is the building block of a large family of flavoproteins. In many of these enzymes, additional domains have been fused to the FNR building block, thus extending the system ability to a wide range of reactions (7, 16).

Coenzyme specificity studies have usually focused in the structural differences between the NADPH and NADH coenzymes, which are reduced to the presence or absence of a phosphate group at the 2' position of the adenine ribose moiety (2'-P-AMP). Although changes limited to the 2'-P or 2'-OH binding pocket in this family of enzymes have proven to be effective in reversing coenzyme specificity in some enzymes (17–19), these changes are usually unable to fully reverse the specificity or cause a dramatic decrease in catalytic efficiency as a side effect (6). This fact soon pointed out that the enzyme residues interacting with regions common to both NADPH and NADH might also be important in conferring coenzyme specificity. Thus, the relevance of the region that binds the pyrophosphate bridge between the 2'-P-AMP and nicotinamide mononucleotide (NMN) moieties of NAD(P)⁺/H has also been demonstrated (6, 20–22).

Apart from these common motifs to any NAD(P)⁺/H binding protein, a new determinant of coenzyme specificity, restricted to the FNR protein family, has been reported. In light of the experimental data and the three-dimensional structures reported for the FNR–NADP⁺ interaction, it is

[†] This work has been supported by the Comisión Interministerial de Ciencia y Tecnología (CICYT, Grant BIO2003-00627 to C.G.-M. and Grant BIO2004-00279 to M.M.) and by CONSI+D (DGA, Grant P006/2000 to M.M.).

* Address correspondence to this author. Fax: +34 976 762123. Phone: +34 976 762476. E-mail: mmedina@unizar.es.

[‡] Universidad de Zaragoza.

[§] Instituto Química-Física Rocasolano. CSIC.

¹ Abbreviations: FNR, ferredoxin–NADP⁺ reductase; FNR_{ox}, FNR in the fully oxidized state; FNR_{rd}, FNR in the hydroquinone state; FNR_{sq}, FNR in the semiquinone state; ET, electron transfer; DCPIP, 2,6-dichlorophenolindophenol; WT, wild type; CP450R, cytochrome P450 reductase; NOS, nitric oxide synthase; NMN, nicotinamide mononucleotide portion of NAD(P)⁺/H; 2'-P-AMP, 2'-phospho-AMP portion of NADP⁺/H; rmsd, root mean square deviation; C-HEGA-10, cyclohexylbutanoyl-*N*-hydroxyethylglucamide.

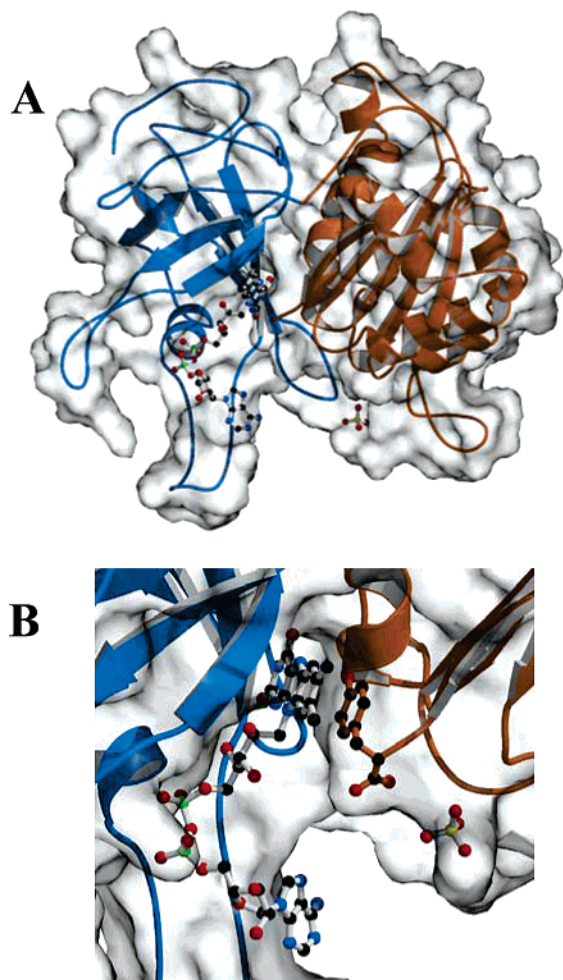


FIGURE 1: Overall structure of native *Anabaena* FNR. (A) Molecular surface and ribbon diagram of the FNR, with the FAD prosthetic group and sulfate ion represented as balls and sticks. Protein binding domains for each cofactor, FAD and NADP⁺, are colored in blue and in orange, respectively. (B) Detail of the FAD binding site showing the FAD, the C-terminal Tyr residue, and sulfate ion in a ball-and-stick representation.

proposed that the last step in optimal coenzyme binding putatively involves displacement of the FNR C-terminal residue (Tyr303 in *Anabaena* FNR, Figure 1B) in order to allow the entrance of the nicotinamide ring into the hydride transfer site (10, 15). This residue can be Tyr, Phe, or Trp in NADP⁺/H binding proteins, whereas in NAD⁺/H-dependent enzymes either a Tyr or a different arrangement of the C-terminus is found (5, 23, 24). Accordingly, the structural features of this C-terminal region in the FNR family of enzymes show two different patterns (see Figure 6 in ref 24). A group of enzymes, such as FNR, cytochrome P450 reductase (CP450R), or nitric oxide synthase (NOS), present an aromatic residue forming a stacking interaction with the isoalloxazine ring of FAD. On the other hand, in most NAD⁺/H-dependent enzymes of the FNR family, the aromatic residue is either absent or occupies a different position, forming a larger cavity around the *re* face of the isoalloxazine ring (24). In this latter case, there would be no need of a side chain displacement in order to accommodate the nicotinamide ring of the coenzyme. Involvement of the C-terminal aromatic residue in coenzyme specificity has been confirmed in pea FNR (5), as well as in other NADP⁺/H-dependent enzymes, such as CP450R (25, 26) or NOS (23).

However, site-directed mutagenesis replacement of this aromatic residue produces different effects in each enzyme, an observation in agreement with the fact that not only coenzyme specificity but other effects such as modification of the reduction potential or inter- and intraprotein ET processes can be affected by the mutation (23, 24).

A closer look at the role of this C-terminal residue is taken in the present work, focusing on the differences found in the interaction with the coenzyme between cyanobacterial FNRs and plant FNRs (27), as well as other members of the FNR family. Thus, structural, spectroscopic, and, especially, fast kinetic (not previously reported for pea FNR variants) studies are here reported for the *Anabaena* FNR Tyr303Phe, Tyr303Trp, and Tyr303Ser interaction and hydride transfer with NAD(P)⁺/H. Such data are discussed in light of previous analysis on these mutants, indicating a role for Tyr303 in modulating the rates of electron exchange with the protein partners by contributing to the flavin semiquinone stabilization required for electron splitting (24), and on those previously reported for related enzymes in order to achieve a deeper understanding of the role of this C-terminal residue in these systems.

MATERIALS AND METHODS

Production of FNR Variants. The Tyr303Ser, Tyr303Phe, and Tyr303Trp *Anabaena* PCC7119 FNR variants were prepared using the construct pET28a-FNR (22) and the QuikChange mutagenesis kit (Stratagene) as previously described (24). The pET28a-FNR vectors carrying the selected mutations were used to transform *Escherichia coli* BL21(DE3) Gold cells (Stratagene). *E. coli* BL21(DE3) Gold cultures carrying the pET28a-FNR plasmid were grown at 30 °C for 24 h. The WT and mutated *Anabaena* FNR forms from the pET28a-FNR vectors were purified as described previously (28). UV-vis spectra and SDS-PAGE were used as purity criteria.

Spectral Analysis. UV-visible spectral measurements were performed in a Kontron Uvikon 942 spectrophotometer. Dissociation constants (K_d) for the complexes of oxidized FNR forms with either NADP⁺ or NAD⁺ were estimated by difference spectroscopy in 50 mM Tris-HCl, pH 8.0, as previously described (6). Errors in the estimated K_d values were $\pm 15\%$.

Enzymatic Assays. Diaphorase activity was assayed using 2,6-dichlorophenolindophenol (DCPIP) as electron acceptor in 50 mM Tris-HCl, pH 8.0 at 25 °C (6). Errors in the estimated values of K_m and k_{cat} were $\pm 20\%$ and $\pm 15\%$, respectively.

Stopped-Flow Kinetic Measurements. Kinetic measurements were performed under anaerobic conditions using an Applied Photophysics SX.17 MV stopped-flow instrument in 50 mM Tris-HCl, pH 8.0 at 25 °C, as previously described (28). Final FNR concentrations were kept between 7 and 9 μM . NADPH and NADH concentrations were in the range of 175–200 μM . Additional measurements were carried out with ~ 2.5 mM NADH. Observed rate constants (k_{obs}) were obtained by fitting the transients to a mono- or biexponential equation. Errors in the estimated values were $\pm 15\%$. Reactions were mainly followed at 460 nm, but other wavelengths, 340 and 600 nm, were also analyzed.

Apparent Equilibrium Constant Calculation. To extract additional information from the experimental dissociation

constants, the global equilibrium was fitted to a hypothetical model in which the binding of the 2'P-AMP and NMN moieties of NADP⁺ are assumed to be independent (see Figure 4 below). For the FNR–NADP⁺ dissociation constants, the experimental values were fitted to the hypothetical scheme which includes both the binding constant $K_{a,2'P-AMP}$ and a second equilibrium constant, K_{in} , which takes into account the concerted movement of the C-terminal residue and the NMN moiety of NADP⁺. The NMN occupancy of the *Anabaena* and pea FNR–NADP⁺ complexes was assumed from spectroscopy and crystallographic data to be 0% and 14%, respectively (5). Thus, for the *Anabaena* WT FNR–NADP⁺ complex, only the C1 species (see Figure 4 below) is formed, and thereby $K_{a,2'P-AMP} = 1/K_d$. The binding of the 2'P-AMP moiety of NADP⁺ was assumed to be similar in WT and mutant FNRs from the same organism, and thus a constant value for $K_{a,2'P-AMP}$ was used. Experimental K_d values (Table 2) were calculated as above-described according to a mechanism that assumes formation of single species, $FNR + NAD(P)^+ \leftrightarrow FNR-NAD(P)^+$. To calculate K_{in} values, the amount of complex formed (calculated using the experimental K_d constant) was assumed to be equal to the sum of the C1 and C2 complexes (see Figure 4 below). In the case of the FNR–NAD⁺ dissociation constants, only the equilibrium involving $K_{a,NMN}$ (see Figure 4 below) is assumed to take place, and then $K_{a,NMN} = 1/K_d$. Calculations were carried out with the Gepasi software, version 3.30 (29). Nicotinamide occupancy calculations are directly derived from the calculated K_{in} values, as in the equilibrium conditions (excess of NADP⁺) all of the FNR is in the form of either the C1 or C2 complexes, and, thus, occupancy (%) = $100[K_{in}/(1 + K_{in})]$.

Crystal Growth, Data Collection, and Structure Refinement. Crystals of the Tyr303Ser and Tyr303Trp FNR variants, and that of the Tyr303Trp and Tyr303Ser FNR variants complexed with NADP⁺, were grown by the hanging drop method. Both Tyr303Ser and Tyr303Trp variants gave hexagonal crystals that grew in 5 μ L droplets consisting of 2 μ L of 0.75 mM protein solution buffered with 10 mM Tris-HCl, pH 8.0, 1 μ L of unbuffered β -octyl glucoside at 5% (w/v), and 2 μ L of reservoir solution containing 18–20% polyethyleneglycol 6000, 20 mM ammonium sulfate, and 0.1 mM MES/NaOH, pH 5.5, or 0.1 mM sodium acetate, pH 5.0. Drops were equilibrated at 20 °C against 1 mL of reservoir solution. Crystals reached their maximum size of 0.8 \times 0.4 \times 0.4 mm in 1–7 days. The Tyr303Trp FNR variant was crystallized complexed with NADP⁺, obtaining tetragonal crystals that grew in 5 μ L droplets formed by 1 μ L of 0.75 mM protein solution buffered with 10 mM Tris-HCl, pH 8.0, 1 μ L of unbuffered C-HEGA-10 solution at 350 mM, and 2 μ L of reservoir solution containing 19% polyethyleneglycol 6000 and 0.1 M sodium acetate, pH 5.0. Complex crystals grew to a maximum size of 0.6 \times 0.02 \times 0.02 mm in about 2 weeks. The complex Tyr303Ser FNR–NADP⁺ was obtained by soaking the crystals of the free protein (crystallized as indicated above) into a 100 mM NADP⁺ solution for 30 min.

The Tyr303Ser and Tyr303Trp crystals belong to the hexagonal $P6_5$ space group with unit cell dimensions that are indicated in Table 1. The V_M are 2.89 and 2.93 $\text{\AA}^3/\text{Da}$ for Ser and Trp variants with one molecule in the asymmetric unit and a solvent content of 60%. Tyr303Trp–NADP⁺

complex crystals belong to the tetragonal $I4$ space group with unit cell dimensions $a = b = 221.3 \text{ \AA}$ and $c = 37.7 \text{ \AA}$. The V_M is 3.20 $\text{\AA}^3/\text{Da}$, and there are two molecules in the symmetric unit with a solvent content of 62%. Tyr303Ser–NADP⁺ complex crystals present unit cell dimensions $a = b = 87.15 \text{ \AA}$ and $c = 96.15 \text{ \AA}$. The V_M is 3.0 $\text{\AA}^3/\text{Da}$ with one molecule in the asymmetric unit and a solvent content of 59%. The X-ray data sets were collected using graphite-monochromated Cu K α radiation generated by Bruker-Nonius rotating anode generators, with a Mar Research imaging plate and Kappa2000 CCD detectors.

Tyr303Ser and Tyr303Ser–NADP⁺ complex X-ray data sets were processed with Mosflm and scaled and reduced with SCALA from the CCP4 package (30). Tyr303Trp and Tyr303Trp–NADP⁺ complex data sets were processed and scaled with Mosflm (31). All of the structures were solved by molecular replacement using the program AMoRe (32) (except that of the Tyr303Ser–NADP⁺ complex, solved using MolRep) on the basis of the native FNR model (PDB code 1QUE) without the FAD cofactor. An unambiguous single solution for the rotation and translation functions was obtained for all proteins. Models were subjected to alternate cycles of refinement with the program CNS (33) and manual model building with the software package O (34).

The Tyr303Ser and Tyr303Trp variant final models consist of residues 9–303 (the first eight residues were not observed in the electron density map), one FAD moiety, one SO₄²⁻ molecule, and solvent molecules. The Tyr303Ser–NADP⁺ and Tyr303Trp–NADP⁺ complexes consist of residues 9–303, one FAD molecule, and one NADP⁺ molecule, and, in the former, also solvent molecules. For the latter, there were not added solvent molecules in the complex model due to the low resolution of the data. The quality of the final structures was assessed with the PROCHECK (35) and WHATCHECK (36) programs. Statistics for refinement are summarized in Table 1. Pictures were generated with MOLSCRIPT (37) and RENDER (38). Atomic coordinates and structure factors for FNR variants have been deposited in the PDB with accession codes 1w34 (Tyr303Ser FNR), 1w35 (Tyr303Trp FNR), 1w87 (Tyr303Trp FNR complexed with NADP⁺), and 2bsa (Tyr303Ser FNR complexed with NADP⁺).

RESULTS

Expression, Purification, and Spectral Properties of FNR Variants. The expression of all of the FNR variants was similar to that of the WT enzyme. The Tyr303Ser and, to a lesser extent, the Tyr303Trp and Tyr303Phe variants were purified with bound NADP⁺ as already reported (10, 24). The nucleotide was removed by chromatography on a Cibacron blue matrix. As previously indicated, the FNR variants showed slight changes in the flavin visible bands (24). The fact that the *Anabaena* Tyr303Ser FNR form is purified in complex with NADP⁺, as also reported for the pea enzyme (5, 10), allows analysis of the spectroscopic characteristics of the Tyr303Ser FNR–NADP⁺ interaction. This spectrum shows a peak displacement of bands I and II of the flavin toward longer wavelengths (not shown), the maxima being shifted from 388 and 456 nm in the NADP⁺-free variant to 401 and 473 nm, respectively, in the Tyr303Ser–NADP⁺ complex. This agrees with the peak

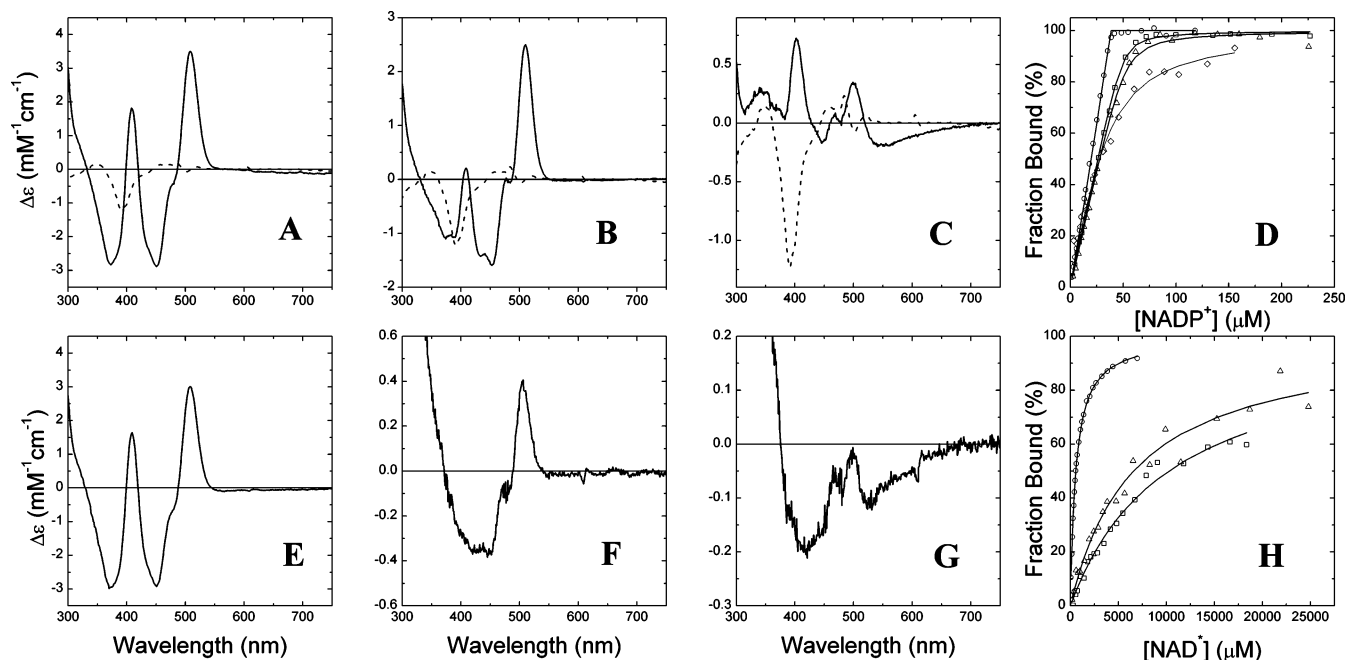


FIGURE 2: Spectroscopic characterization of the complexes between the *Anabaena* FNR_{ox} forms and the coenzymes NADP⁺ and NAD⁺. (A–C) Difference spectra elicited by the binding of (A) Tyr303Ser and NADP⁺, (B) Tyr303Phe and NADP⁺, and (C) Tyr303Trp and NADP⁺ (solid lines). The difference spectrum elicited by the binding of WT FNR and NADP⁺ is shown in panels A–C as a dashed line. (D) Spectrophotometric titration of the FNR WT and mutant enzymes with NADP⁺: WT enzyme (open diamonds, thin line); Tyr303Ser (open circles); Tyr303Phe (open squares); Tyr303Trp (open triangles). (E–G) Difference spectra elicited by the binding of (E) Tyr303Ser and NAD⁺, (F) Tyr303Phe and NAD⁺, and (G) Tyr303Trp and NAD⁺. (H) Spectrophotometric titration of the FNR variants with NAD⁺: Tyr303Ser (open circles); Tyr303Phe (open squares); Tyr303Trp (open triangles).

displacement reported for the pea Tyr308Ser–NADP⁺ complex (10). Noticeably, the Tyr303Trp variant shows a broad band I with absorbance far beyond 550 nm (see Figure 1 from ref 24). A similar effect in band I has been observed in other flavoproteins with a Trp side chain in the close environment of the isoalloxazine ring, as in the Tyr94Trp variant of *Anabaena* PCC7119 flavodoxin (39), and the WT CP450R, where a tryptophan residue occupies the equivalent position of Tyr303 in *Anabaena* FNR (40). Extension of band I to longer wavelengths has been assigned to a charge transfer character of the interaction between the Trp and the isoalloxazine moiety of the flavin.

Interaction of the FNR Variants with NADP⁺ and NAD⁺. The ability of the different FNR variants to interact with NADP⁺ and/or NAD⁺ was analyzed by difference spectroscopy. Addition of both pyridine nucleotides elicited difference spectra for all of the FNR mutants, indicating complex formation with both coenzymes and allowing determination of the corresponding K_d values (Figure 2). The main feature observed in the difference spectra of WT *Anabaena* FNR upon NADP⁺ titration is a valley around 390 nm (dotted line in Figure 2A–C). Noticeably, different difference spectra were obtained for the three *Anabaena* FNR variants upon addition of NADP⁺, all of them showing a prominent peak in the 500–510 nm region (solid line in Figure 2A–C). Such peak has previously been reported as an indication of a stacking interaction of the NADP⁺ nicotinamide ring with the isoalloxazine ring of FAD in higher plant FNRs but never before seen in the case of cyanobacterial FNRs, including *Anabaena* (5, 10, 27). Difference spectra of the Tyr303Ser and Tyr303Phe variants elicited by NADP⁺ show similar maxima and minima (maxima at 409 and 508 nm, minima at 373 and 450 nm), with differences of ± 2 nm (Figure 2A,B). The Tyr303Phe difference spectrum shows a smaller

$\Delta\epsilon$ in the 409 nm peak (Figure 2B) and a better resolution in the valleys, with additional minima at 390 and 433 nm. The difference spectra of the Tyr303Trp–NADP⁺ complex show distinctive and interesting features (Figure 2C). Thus, although binding of NADP⁺ to this FNR variant is considerably tight, as assessed by its K_d value (Table 2), the shape of the spectrum suggests a different relative arrangement of the isoalloxazine and nicotinamide rings. Comparison to the difference spectra of the Tyr303Ser and Tyr303Phe variants shows changes in both the intensity and the wavelength of the maxima and minima. The spectrum shows maxima at 402 and 499 nm and minima at 380, 447, and 542 nm (Figure 2C). The peaks are thus displaced to shorter wavelengths, as in the visible spectrum of the free enzyme. The $\Delta\epsilon$ of the difference spectrum is much smaller, suggesting a lesser occupancy of the nicotinamide binding site and/or a different binding mode. However, the most remarkable feature in the difference spectra is the loss of absorbance observed at wavelengths over 525 nm that corresponds to the loss of the broad band of the visible spectrum of the unbound FNR variant upon NADP⁺ binding. Since this band has been related to a Trp/isoalloxazine ring charge transfer interaction (24), its absorbance decrease must be related to a disruption of such interaction. This strongly suggests a rearrangement in which the Trp303 side chain moves away to allow the nicotinamide ring entrance into the catalytic site, as has been proposed to happen to the Tyr in the WT enzyme (10, 15).

The K_d values obtained for the complexes of the mutated forms with NADP⁺ are in all cases smaller than that reported for the WT enzyme, indicating a higher affinity toward the coenzyme (Table 2). Tyr303Trp and Tyr303Phe showed a 3.5- and 5-fold decrease of the K_d values, whereas the affinity of the Tyr303Ser variant for NADP⁺ is extremely high and only an upper limit for the K_d value could be estimated

Table 1: Experimental Data for Variant and Complexed Crystal Structures

	Tyr303Ser	Tyr303Trp	Tyr303Trp–NADP ⁺	Tyr303Ser–NADP ⁺
crystal data				
space group	<i>P</i> 6 ₅	<i>P</i> 6 ₅	<i>I</i> 4	<i>P</i> 6 ₅
<i>a</i> , <i>b</i> (Å)	86.3	87.1	221.3	87.2
<i>c</i> (Å)	96.7	96.2	37.7	96.8
data collection statistics				
wavelength (Å)	1.5418	1.5418	1.5418	1.5418
resolution (Å) ^a	23.0 (1.82)–1.73	32.3 (1.97)–1.90	35.0 (3.1)–3.0	27.3 (2.02)–1.92
unique data	42423	32488	16780	31825
redundancy	4.6 (4.3)	9.6 (5.0)	5.0 (2.6)	12.1 (10.8)
completeness (%)	99.4 (97.5)	100 (100)	88.2 (58.2)	99.7 (99.7)
<i>I</i> / σ (<i>I</i>)	6.7 (2.9)	14.0 (3.0)	6.8 (1.6)	8.5 (2.6)
<i>R</i> _{sym}	0.06 (0.24)	0.14 (0.35)	0.17 (0.60)	0.071 (0.29)
refinement statistics				
resolution range (Å)	23.0–1.73	32.3–1.90	35.0–3.0	27.3–1.92
<i>R</i> _{work} (<i>R</i> _{free})	0.18 (0.20)	0.17 (0.20)	0.23 (0.27)	0.20 (0.22)
rmsd bonds (Å)	0.006	0.007	0.011	0.009
rmsd angles (deg)	1.4	1.3	1.7	1.5
no. of atoms	2832	2889	4880	2708
protein	2331	2339	4678	2429
water	443	492	0	278
FAD	53	53	106	53
NADP ⁺			96	48
SO ₄ ²⁻	5	5		

^a Highest resolution shell is shown in parentheses.

Table 2: Dissociation Constants and Extinction Coefficient Changes at Selected Wavelengths for Complex Formation between Different FNR Forms in the Oxidized State and NADP⁺ or NAD⁺

FNR form	<i>K</i> _d ^{NADP⁺} (μM)	Δε (mM ⁻¹ cm ⁻¹)	λ ^d (nm)	<i>K</i> _d ^{NAD⁺} (μM)	Δε (mM ⁻¹ cm ⁻¹)	λ ^d (nm)
WT ^a	5.7 ± 0.3	1.2 ± 0.1	393	ND ^b	ND ^b	ND ^b
Tyr303Phe	1.2 ± 0.16	2.5 ± 0.1	510	10200 ± 1100	0.4 ± 0.05	504
Tyr303Trp	1.6 ± 0.6	0.35 ± 0.02	499	6100 ± 800	0.02 ± 0.004	420
Tyr303Ser	<<0.01 ^c	3.5 ± 0.1	509	550 ± 20	3.0 ± 0.2	507

^a Data from ref 28. ^b No difference spectra were detected. ^c Exact value cannot be accurately determined. ^d Wavelength at which Δε is calculated.

(Figure 2D). Extinction coefficients were calculated for the peak in the 500–510 nm region, which is related to the nicotinamide occupancy of the putative ET site (5, 10) (Table 2). The values indicate a very high occupancy for the Tyr303Ser and Tyr303Phe variants (100% and ~75%, respectively). The Tyr303Trp variant might present an occupancy over 60%, as calculated indirectly (see below, Table 5), but the observed spectral changes precluded direct comparison to the Tyr303Ser and Tyr303Phe variants.

Whereas WT FNR is unable to form any complex with NAD⁺ as judged by difference spectroscopy (6, 27), NAD⁺ addition elicited difference spectra for all of the FNR variants here studied (Figure 2E–G), allowing determination of the corresponding dissociation constants (Figure 2H). As expected, these *K*_d values were much higher than those obtained with NADP⁺ (Table 2). The spectral features of the Tyr303Ser–NAD⁺ complex (Figure 2E) are almost identical to those of the complex with NADP⁺, suggesting a flavin–nicotinamide interaction similar in both cases, albeit weaker with NAD⁺ (Table 2). The Tyr303Phe and Tyr303Trp variants showed weak difference spectra upon NAD⁺ titration (Figure 2F,G). Both spectra show a broad valley between 400 and 475 nm, roughly similar to that reported for the FNR–NAD⁺ complexes of the FNR variants Leu263Pro and Leu263Ala (see Figure 2 in ref 22). The Tyr303Phe variant still presents a measurable amount of nicotinamide–flavin interaction, as judged by the peak of 504 nm (Figure 2F). NAD⁺ addition to Tyr303Trp elicited a weak difference spectrum, but the small peak at 494 nm and the absorption

decrease in the long wavelength range indicate that the main features of the Tyr303Trp–NADP⁺ interaction are conserved. The calculated parameters indicate a weak, but measurable, interaction with NAD⁺ for the Tyr303Phe and Tyr303Trp variants, with *K*_d values in the millimolar range and a 6- and 17-fold decrease in the Δε with regard to the NADP⁺ interaction. On the other hand, removal of the aromatic residue in the Tyr303Ser variant causes an enhancement of the NAD⁺ affinity, with almost complete occupancy of the putative nicotinamide binding site as indicated by the Δε value (Table 2).

Steady-State Kinetics of the FNR Variants. The diaphorase activity of the different FNR variants was assayed with DCPIP as artificial electron acceptor and either NADPH or NADH as electron donor (Table 3). All variants showed an enhanced affinity for NADPH, with *K*_m decreasing between 2- and 8-fold. Replacement of the C-terminal Tyr by Ser leads to a variant with a considerably decreased *k*_{cat} value, whereas the Tyr303Phe and Tyr303Trp variants show *k*_{cat} values similar to that of the WT enzyme. A similar behavior was reported for the pea enzyme (5). Therefore, higher catalytic efficiency, as judged by the *k*_{cat}/*K*_m ratio (2- and 6-fold increase for Tyr303Phe and Tyr303Trp, respectively), is achieved, with the only exception of Tyr303Ser (Table 3). Thus, in the case of the Tyr303Ser variant, the affinity enhancement causes a slow release of the product, which becomes the rate-limiting step (5). The introduced mutations produced a considerable enhancement of the NADH-dependent activity. Thus, although only the Tyr303Ser variant

Table 3: Steady-State Kinetic Parameters for Diaphorase Activity with DCPIP of WT and Mutant FNR Forms

FNR form	$K_m(\text{NADPH})$ (μM)	$k_{\text{cat}}(\text{NADPH})$ (s^{-1})	$k_{\text{cat}}/K_m(\text{NADPH})$ ($\text{s}^{-1}\cdot\mu\text{M}^{-1}$)	$K_m(\text{NADH})$ (μM)	$k_{\text{cat}}(\text{NADH})$ (s^{-1})	$k_{\text{cat}}/K_m(\text{NADH})$ ($\text{s}^{-1}\cdot\mu\text{M}^{-1}$)	specificity ^a
WT ^b	6.0	81.5	13.5	800	0.16	2×10^{-4}	67500
Tyr303Phe	3.4	99	29	780	41	5.3×10^{-2}	550
Tyr303Trp	0.78	63	81	770	4.9	6.4×10^{-3}	12600
Tyr303Ser	1.1	2.8	2.5	48	93	1.9	1.3

^a Defined as the ratio $[k_{\text{cat}}/K_m(\text{NADPH})]/[k_{\text{cat}}/K_m(\text{NADH})]$. ^b Data from ref 28.

shows a significant decrease (16-fold) of the K_m for NADH with regard to the WT, whereas Tyr303Phe and Tyr303Trp present K_m values similar to WT, the k_{cat} values are increased by 30-, 250-, and 580-fold in the Tyr303Trp, Tyr303Phe, and Tyr303Ser variants, respectively. These changes lead to a 30-, 260-, and 9500-fold efficiency increase in the reaction with NADH.

It is interesting to note that the FNR variants with the lower k_{cat} values in the NADPH-dependent reaction turned out to be the ones displaying the highest NADH-dependent activities (Table 3). In the latter reaction, the Tyr303Ser variant showed a k_{cat} value 3 orders of magnitude higher than that of the WT enzyme and comparable with the k_{cat} of the WT FNR with NADPH as a substrate. The Tyr303Phe variant, which was very efficient as an NADPH-dependent catalyst, also showed a remarkably high k_{cat} in the NADH-dependent reaction. Additionally, the K_m of FNR for NADH was indeed affected by mutations of the C-terminal residue with a pattern similar to that observed for NADPH. Whereas substituting Tyr by Phe or Trp did not produce major changes in the K_m value for NADH, replacement by Ser caused a decrease in the K_m as compared with the WT value (Table 3). Such behavior is observed in the case of the Tyr303Ser variant for both coenzymes, but binding of NADPH is 43-fold much stronger than binding of NADH. These data, in combination with the corresponding ones in Table 2, suggest that, after the hydride transfer takes place, release of NAD^+ from the Tyr303Ser variant to initiate a new cycle is much easier than release of NADP^+ , being this event, and not the hydride transfer itself, the rate-limiting step in the catalytic mechanism with NADPH (as will be confirmed below by stopped-flow data). These observations strongly support the idea that the decrease in k_{cat} for the NADPH-dependent diaphorase reaction of the Ser mutants was caused by tight binding of the NADP^+ product during enzyme turnover (5).

To assess the relative change in the specificity, the $[k_{\text{cat}}/K_m(\text{NADPH})]/[k_{\text{cat}}/K_m(\text{NADH})]$ ratio was calculated (6, 20) (Table 3). The large increases in NADH efficiency yield a change of the specificity for NADPH from the 67500 value of the WT enzyme to a value of just 1.3 for the Tyr303Ser variant, which is virtually unable to distinguish between both coenzymes.

Stopped-Flow Kinetic Analysis of the Reaction of the FNR Variants with either NADPH or NADH. The fast kinetics of the reaction between the FNR variants and either NADPH or NADH was followed using stopped-flow anaerobic techniques (Figure 3 and Table 4). Flavin reduction by hydride transfer was monitored by following the decrease in absorbance at 460 nm, and the observed kinetics were compared with those reported for the WT enzyme (6, 28). In most cases, reactions were best fit to a biphasic process, with a fast step related to the formation of a charge transfer

complex $[\text{FNR}_{\text{ox}}-\text{NADPH}]$ followed by the hydride transfer and the fast equilibration of a mixture of both charge transfer complexes, $[\text{FNR}_{\text{ox}}-\text{NADPH}]$ and $[\text{FNR}_{\text{rd}}-\text{NADP}^+]$, as reported for the spinach and *Anabaena* WT enzymes (28, 41, 42).

Reaction of all FNR variants with NADPH was a considerably fast process, although the observed rate constants (k_{obs}) were slightly lower than those reported for WT FNR (Figure 3A and Table 4). Thus, reaction was very fast for the Tyr303Ser and Tyr303Phe variants, with most of the absorbance decrease occurring within the instrumental dead time, whereas a much longer portion of the process can be followed for the reaction with the Tyr303Trp variant (Figure 3A). The Tyr303Trp variant yielded a slightly slower kinetics, and its transient was best fit to a monoexponential process. However, the k_{obs} decrease was no more than 3-fold. Analyses of the kinetic traces at 600 nm (data not shown) showed a slight absorbance decay, but due to the very small amplitude of the changes, interpretation of these data has not been attempted.

The behavior of the variants in the reaction with NADH was very different from that reported for the WT enzyme. Reaction rates were much higher, with k_{obs} increases of 14-, 120-, and up to 1400-fold for Tyr303Trp, Tyr303Phe, and Tyr303Ser, respectively (Table 4 and Figure 3B–D). Thus, reduction of Tyr303Ser by NADH reaches k_{obs} values in the range of those obtained for the reduction of the WT enzyme by NADPH and shows a small dependency on the NADH concentration (Figure 3B). The Tyr303Phe and Tyr303Trp variants show a much higher dependency on the NADH concentration (Table 4), probably related to the much lower affinity of these FNR variants toward NADH as compared to the Tyr303Ser variant. Kinetic traces for the Tyr303Phe variant were best fit to a monoexponential process, but Tyr303Trp clearly shows a biphasic character. Reactions of Tyr303Phe and Tyr303Trp with NADH showed a decrease at 340 nm that resembles the data at 460 nm (insets in Figure 3C,D). This strongly indicates that the rates obtained at 460 nm indicate hydride transfer from NADH to the flavin ring, whereas this is not usually the case in the reactions with NADPH, where intermediate complex formations might account for changes in absorbance at 460 nm but not at 340 nm. The main feature of the traces obtained at 600 nm (Figure 3D, inset) is the absorbance increase for the Tyr303Trp variant. As these changes appear at time scales beyond 2 s, and there is no concomitant NADH oxidation as assessed by the absence of absorbance changes at 340 nm (Figure 3D, inset), it may be related to a secondary reaction such as deproportionation of FNR_{ox} and FNR_{rd} to form FNR_{sq} .

It is worth noting that, unlike the majority of the reactions of the WT and variants with the coenzymes, reactions of

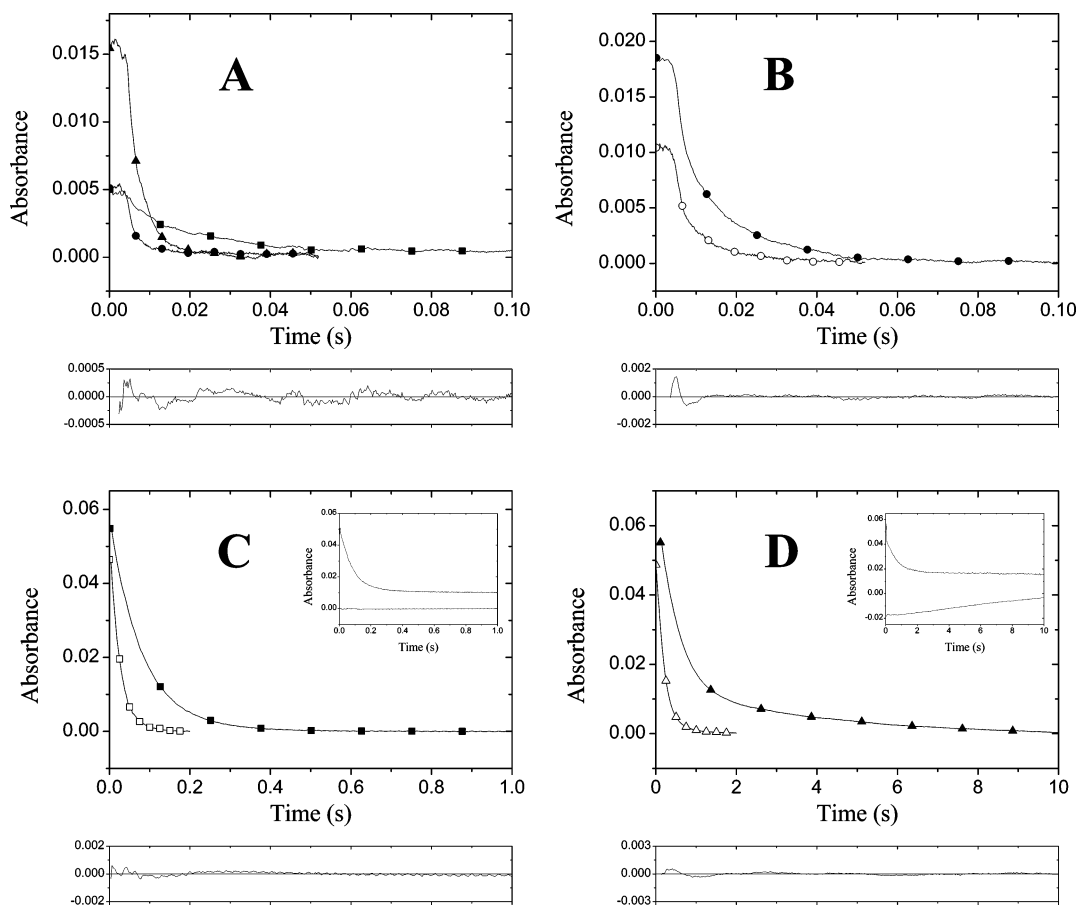


FIGURE 3: Time course of the anaerobic reactions of the different FNR forms with NADPH and NADH followed by stopped-flow analysis. (A) Reaction with NADPH. Kinetic traces for the reaction of Tyr303Ser (6.9 μM) with NADPH (190 μM) (filled circles), Tyr303Phe (7.8 μM) with NADPH (200 μM) (filled squares), and Tyr303Trp (8.9 μM) with NADPH (175 μM) (filled triangles). (B) Reaction of Tyr303Ser (7.0 μM) with NADH, 170 μM (filled circles) and 2.5 mM (open circles). (C) Reaction of Tyr303Phe (7.8 μM) with 190 μM NADH (filled squares) and 1.8 mM NADH (open squares). Inset: Kinetic traces at 340 nm (upper trace) and 600 nm (lower trace) for the reaction of Tyr303Phe with 190 μM NADH. (D) Reaction of Tyr303Trp (8.3 μM) with 180 μM NADH (filled triangles) and 2.4 mM NADH (open triangles). Inset: Kinetic traces at 340 nm (upper trace) and 600 nm (lower trace) for the reaction of Tyr303Trp with 180 μM NADH. Final concentrations are given. Residual plots for selected fittings are shown underneath.

Table 4: Fast Kinetic Parameters for Reduction of Different FNR Forms by NADPH and NADH As Obtained by Stopped-Flow Analysis

FNR form	NADPH		NADH	
	$k_{\text{obs}1}$ (s^{-1})	$k_{\text{obs}2}$ (s^{-1})	$k_{\text{obs}1}$ (s^{-1})	$k_{\text{obs}2}$ (s^{-1})
WT	>500	200	0.35 ^a	0.005 ^a
Tyr303Phe	>500	64	12.3	N/A ^b
Tyr303Trp	270	N/A ^b	41.3 ^a	N/A ^b
Tyr303Ser	460	18.8	1.7	0.16
			4.96 ^a	0.485 ^a
			420	67
			>500 ^a	105 ^a

^a Reactions with 2.5 mM NADH (final concentration). ^b The stopped-flow data for these reactions were fitted to a single-exponential equation.

Tyr303Phe with NADH and Tyr303Trp with NADPH were best fitted to monoexponential processes. The observed changes in absorbance reflect the association and inter-conversion of the NAD(P)H–FNR forms, processes that can take place at different rates for the different FNR variants, involving each of the various reported k_{obs} values of these processes. Therefore, changes in the number of fitted processes not necessarily mean a change in the overall reaction mechanism but rather a change in the mean life of the reaction intermediate species. Therefore, thus far, we do not have a mechanistic explanation for the observation here

presented. Nevertheless, further work along these lines is underway in the FNR system by using photodiode array detection and singular value deconvolution methods and will be reported elsewhere.

Crystal Structure of the Tyr303Trp and Tyr303Ser Anaerobically Reduced FNR Variants. The three-dimensional structures of the Tyr303Trp and Tyr303Ser FNR variants were solved by molecular replacement and refined up to 1.9 and 1.7 Å resolution, respectively. The first eight residues in the sequence were not observed in the electron density map in none of the mutant FNR structures, similarly to that reported for other FNR crystal structures (28). The overall folding of these FNR variants shows no significant differences with respect to the native FNR, as shown by the rmsd of the C α backbones (0.33 and 0.35 Å for the Tyr303Trp and Tyr303Ser FNR variants, respectively).

With regard to the Tyr303Trp variant (Figure 5A), the Trp303 side chain is stacking to the isoalloxazine ring, as Tyr303 in the native structure. Prominent differences are only found in the Tyr303Ser FNR variant that shows a poorly defined electron density in the last three residues of the C-terminus (Figure 5B) and in loop 261–267 close to it. This loop not only seems to be disordered but also shows a conformational change with respect to the native enzyme that mainly consists of a readjustment of Leu263 which, in

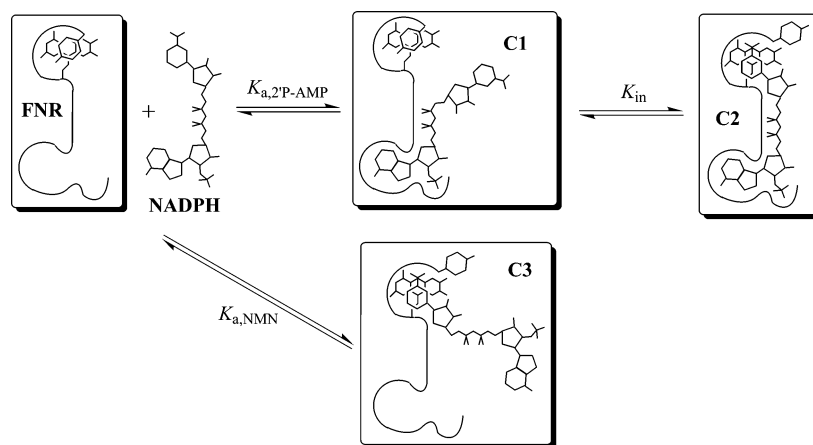


FIGURE 4: Proposed scheme for NAD(P)⁺/H binding to FNR. C1 designates a complex similar to that reported by Hermoso et al. (15), with the pyrophosphate, adenine, and 2'-P bound to FNR. C2 resembles a complex in disposition suitable for hydride transfer. When the affinity of the enzyme for the 2'-P is low or the affinity for the nicotinamide ring is too high, nucleotide binding can be driven by C3. See text for details.

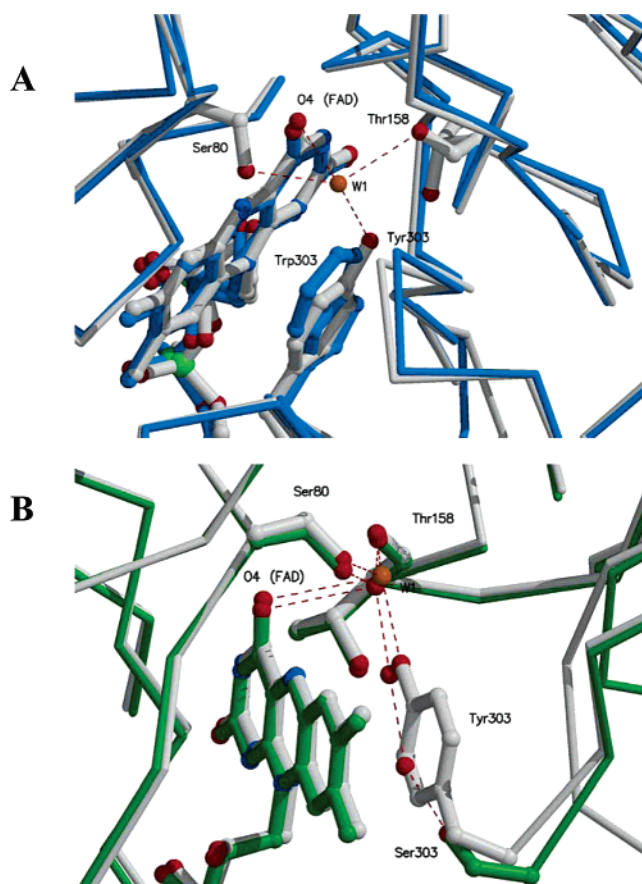


FIGURE 5: Structural changes upon Tyr303 mutation. (A) Structural superimposition of native FNR (white) and the Tyr303Trp variant (blue). The FAD cofactor and the C-terminal residues are represented as balls and sticks. The conserved water molecule (W1) in native FNR is colored in orange. (B) Structural superimposition of native FNR (white) and the Tyr303Ser variant (green). The water hydrogen bond network (see text) is also represented.

the native FNR, orients its side chain to the NADP⁺/H binding site, while in this variant it is oriented to the interior of the protein, increasing the size of the cavity. The disorder in this region may be due to the mutation of the Tyr303 by Ser as, in the native structure, the loop 261–267 H-bonds to the C-terminal residues that are in turn stabilized by stacking interactions of the Tyr303 side chain to the

isoalloxazine ring. Therefore, the Tyr303Ser replacement disturbs a number of stabilizing interactions at the C-terminus of the polypeptide chain that also extend to the 261–267 loop. Additionally, the smaller side chain at the C-terminus makes an enlarged nicotinamide binding site. Some other differences in the active site of both variants have been observed with respect to the native structure, particularly concerning a highly conserved water molecule (W1) (9). This water molecule is stabilized by H-bonds to several residues, including the OH group of Tyr303 (Figure 5A), and has been proposed to be acting as a proton donor to the N5 of the isoalloxazine ring (8). This W1 has not been found in the Tyr303Trp variant. In the case of the Tyr303Ser variant, W1 is conserved, and there are also two additional water molecules occupying the C-terminal Tyr site (Figure 5B). One of these additional water molecules is mimicking the Tyr303 hydroxyl group of the native structure, and the other is placed just in the middle of the aromatic ring. Then, they are forming a H-bond network from the Ser303 hydroxyl group to the W1.

Crystal Structure of the Tyr303Trp and Tyr303Ser FNR Variants in Complex with NADP⁺. Cocrystallization of the Tyr303Trp FNR variant with NADP⁺ produces tetragonal crystals nonisomorphous to native. The structure solved by molecular replacement presents two molecules in the asymmetric unit, and the electron density map showed a strong density for both complete NADP⁺ molecules. The complex structure has been refined up to 3.0 Å resolution. The overall FNR folding is equivalent to that of the free *Anabaena* FNR, and no significant changes in the relative orientation of the FAD and NADP⁺ domains were observed, with the rmsd of the C α backbones being 0.57 Å. The NADP⁺ molecule is placed in the cavity located at the C-terminal edge of the parallel β -sheet of the NADP⁺ binding domain, which extends toward the FAD binding domain interface (Figure 6A). The coenzyme presents an L-shape conformation as was observed in the native FNR complexed with NADP⁺ (15), where the pyrophosphate group is located at the corner and the two branches of the L were accommodating the NMN and 2'-P-AMP moieties, respectively (Figure 6B). Similarly to the reported FNR–NADP⁺ complex (15) the adenine of the AMP moiety is sandwiched between the hydrophobic Leu263 side chain and the aromatic ring of Tyr235 and is

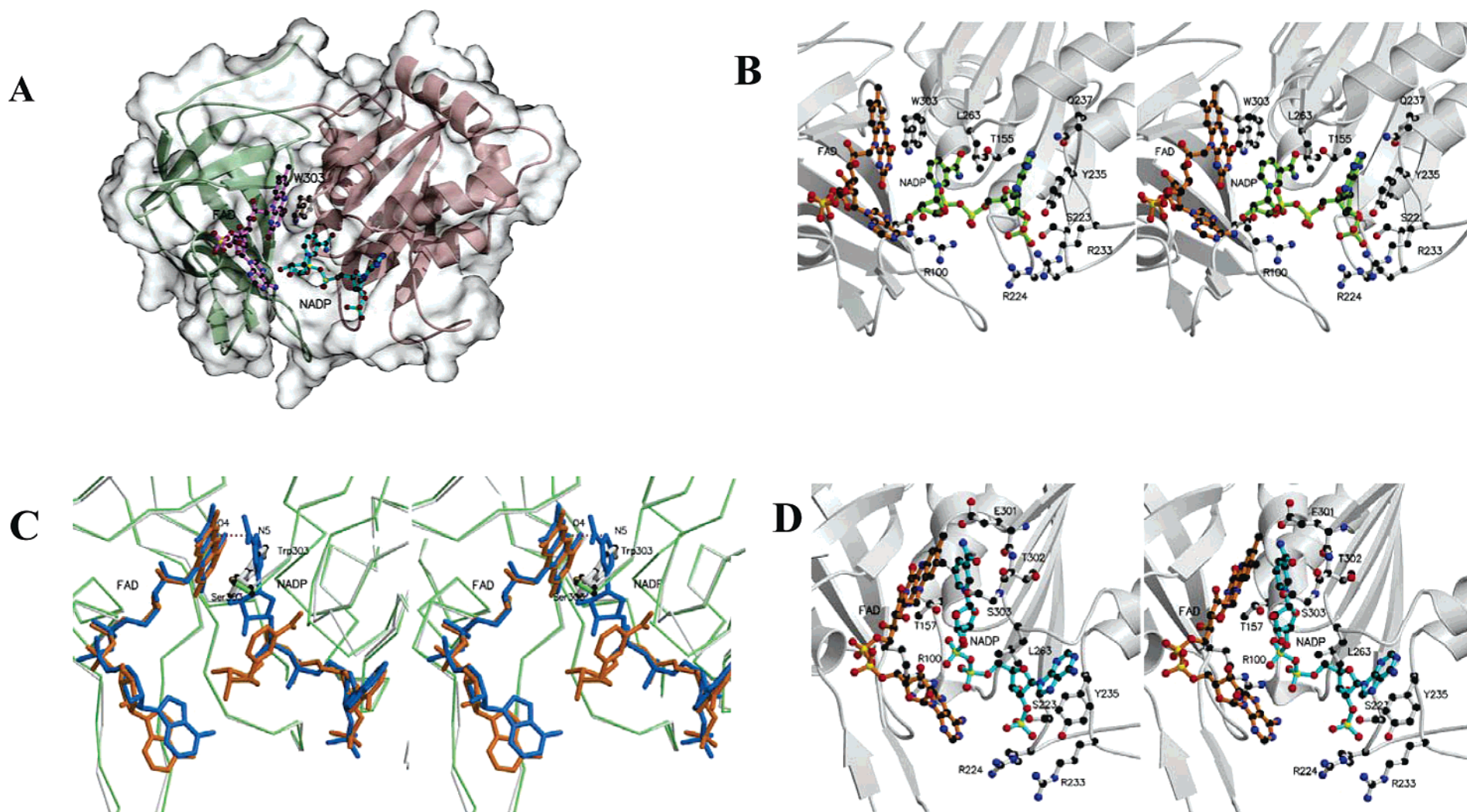


FIGURE 6: Crystal structures of Tyr303Trp FNR–NADP⁺ and Tyr303Ser FNR–NADP⁺ complexes. (A) Molecular surface and ribbon diagram of the Tyr303Trp FNR–NADP⁺ complex. The FAD prosthetic group (pink), NADP⁺ coenzyme (cyan), and Trp303 (purple) are represented as balls and sticks. Protein binding domains for each cofactor, FAD and NADP⁺, are colored pale green and purple, respectively. (B) Stereo diagram showing the residues lining the NADP⁺ in the Tyr303Trp FNR–NADP⁺ complex. Relevant residues are shown in a ball-and-stick representation and colored by atom type. FAD (orange) and NADP⁺ (green) cofactors are drawn in a ball-and-stick representation. (C) Stereoview representation of the superimposition of Tyr303Trp FNR–NADP⁺ (white) and Tyr303Ser FNR–NADP⁺ (green) complexes. FAD cofactor and NADP⁺ coenzyme are colored in orange for the Tyr303Trp FNR and in blue for the Tyr303Ser FNR. (D) Stereo diagram showing the residues lining the NADP⁺ in the Tyr303Ser FNR–NADP⁺ complex. Relevant residues are shown in a ball-and-stick representation and colored by atom type. FAD (orange) and NADP⁺ (cyan) cofactors are drawn in a ball-and-stick representation.

also making an H-bond with the Gln237 side chain. The 2'-P group of the NADP⁺ is stabilized by several H-bonds with the side chains of Ser223, Arg224, and Arg233 and the OH group of the Tyr235. The pyrophosphate moiety of NADP⁺ is essentially stabilized by the guanidinium group of Arg100. The NMN moiety is only stabilized by two polar interactions with Thr155 and by van der Waals contact with Leu263. Trp303 is stacked between the isoalloxazine and the nicotinamide rings, the latter one presenting its B-face to the *re* face of the FAD, and therefore, it is not orientated properly according to the specificity defined for FNR (43). It is remarkable that although the nicotinamide ring is placed close to the isoalloxazine, it does not replace the C-terminal Trp, as previously reported for pea FNR (10).

Unlike the Tyr303Trp FNR variant, the complex of the Tyr303Ser FNR variant with NADP⁺ was obtained by soaking the FNR variant crystals into a NADP⁺ solution, as cocrystallization trials rendered crystals of poor quality. The structure was solved by molecular replacement, and the electron density maps clearly showed density for a NADP⁺ molecule. The crystal structure has been refined up to 1.9 Å resolution and presents one single molecule in the asymmetric unit. The overall FNR folding shows no significant differences with respect to the native and the Tyr303Ser variant structures, as demonstrated by the low rmsd of the C α backbone (0.29 for native FNR and 0.34 for Tyr303Ser FNR). Overall, only slight differences are observed out of the NADP⁺ binding region in loop 104–113, but they are not significant due to the poor definition of the electron density map in this region for all FNR forms. In this complex, NADP⁺ presents a different conformation from that described above for the Tyr303Trp FNR variant complex (Figure 6C). The nicotinamide binds with its A-side facing the *re* face of the central ring of the isoalloxazine, which is consistent with the stereochemistry of hydride transfer reported for this enzyme. The C4 atom of nicotinamide and the N5 atom of FAD are 3.4 Å apart, an arrangement that appears reasonable for direct hydride transfer. The same conformation of the NADP⁺ has been previously described in the complexes of Tyr308Ser and Tyr308Trp pea FNR variants with NADP⁺ (10). As in these pea complexes, the nicotinamide and the isoalloxazine rings are not parallel. They align with an angle of $\sim 30^\circ$, with the C4 atom of the nicotinamide being the closest to the isoalloxazine ring and the N1 of the nicotinamide the farthest (4.6 Å from the FAD C10 atom). In addition, the carboxamide group is stabilized by hydrogen bonds with the side chains of residues Glu301 and Ser303. The latter also makes an H-bond with the 2'-hydroxyl of the nicotinamide ribose.

Concerning the pyrophosphate and the AMP moieties of NADP⁺, they bind in a similar way to that in the complexes of the native and Tyr303Trp FNR variant with NADP⁺ and also to the corresponding complexes from Tyr308Ser and Tyr308Trp pea variants. However, some differences are remarkable in the Tyr303Ser FNR–NADP⁺ complex. Thus, although the adenine is still sandwiched between the side chains of Leu263 and Tyr235, the conformation of the Tyr ring remains in the complex the same as that in the free protein and forms an angle of $\sim 52^\circ$ with the adenine of the NADP⁺ (Figure 6D). Finally, the side chains of Arg224 and Arg233 are in this complex farther from the 2'-P group of the AMP moiety (3.82 Å for Arg224 and 3.91 Å for Arg233)

than in the analogous pea complex Tyr308Ser–NADP⁺ (3.51 for Arg 229 and 2.94 for Lys238).

DISCUSSION

Most enzymes of the FNR family present an aromatic residue, usually at the C-terminus, which forms a parallel π – π stacking interaction with the FAD isoalloxazine ring. Removal of this residue has been shown to allow productive binding of the NMN moiety of NADP⁺ (10, 40), in agreement with the hypothesis stating that a conformational change of this aromatic side chain is required for proper coenzyme binding prior to hydride transfer (8). Various studies have been reported at the C-terminus of FNRs from different species (5, 10, 24, 44) and at the equivalent residue of CP450R (25, 26, 40, 45, 46) and NOS (23, 47). However, although experimental evidence of the function of this residue in some members of the FNR family has been reported (45, 46), there is not complete agreement on the issue yet, and as recently pointed out, the role of this C-terminal aromatic residue still “remains a mystery” for some proteins (48). To further address the study of such uncertainty, we have analyzed the effect of mutations of the Tyr303 residue in *Anabaena* FNR in the processes with NAD(P)⁺/H by analyzing effects in steady-state kinetics, fast kinetics, and complex formation from either the structural or biochemical points of view. The obtained data in the cyanobacterial enzyme are compared with those previously reported for plant-type FNRs.

Structural and difference spectroscopy data implied that NADP⁺/H binds to FNR in such a way that the two moieties of the dinucleotide can bind to the enzyme in a partially independent way (15). In WT FNR, the FNR–NADP⁺ complex is mainly stabilized by interactions involving the 2'-P-AMP moiety of the dinucleotide, whereas the nicotinamide ring does not contribute significantly to the binding energy (42). Thus, in the NADP⁺/H complex of WT FNR, the 2'-P-AMP moiety fully occupies its binding site, whereas the NMN moiety binds at a very low occupancy. The latter complex is destabilized because the energetic cost of displacing the C-terminal Tyr side chain outweighs the energetic gain due to nicotinamide binding (10). Slight, but important, differences can be found between *Anabaena* and higher plant WT enzymes with regard to their action mechanisms with the coenzyme due to the NMN occupancy of the active site. Differential spectroscopy studies indicate that although *Anabaena* and pea FNRs present a similar affinity for NADP⁺ (5, 6, 27), different interactions between the isoalloxazine ring and the nicotinamide ring are present. In the case of the cyanobacterial enzymes, the difference spectra elicited with either NADP⁺ or 2',5'-ATP-ribose are essentially the same (27), suggesting that the observed spectral changes are due to the binding of the 2',5'-ADP moiety of NADP⁺ to FNR. Thus, the NMN moiety does not appear to enter the FAD environment in the interaction of NADP⁺ with the native cyanobacterial enzyme. This is not the case for the higher plant FNRs or the *Anabaena* FNR variants here studied, which show a difference spectrum with a peak around 510 nm related to the interaction of the nicotinamide ring of NADP⁺ with the isoalloxazine moiety of FAD (5, 10). Such observations clearly indicate higher occupancy by the NMN moiety of NADP⁺/H of the FNR active site and interaction between the flavin ring and the

Table 5: Calculated Equilibrium Constants for Bipartite Binding of Nicotinamide Coenzymes^a

FNR form	$K_{a,2P-AMP}$ (μM^{-1})	K_{in}	$K_{a,NMN}$ (μM^{-1})	% occ _{exp} ^b	% occ _{calc} ^b
<i>Anabaena</i> PCC7119					
WT	0.175	<0.01	$\ll 1.0 \times 10^{-4}$	0	0
Tyr303Phe	0.175 ^c	3.7	1.0×10^{-4}	71	79
Tyr303Trp	0.175 ^c	2.6	1.6×10^{-4}	~15	71
Tyr303Ser	0.175 ^c	>50	1.8×10^{-3}	100	>98
pea					
WT	0.093	0.16	$\ll 1.0 \times 10^{-4}$	14 ^d	14 ^e
Tyr308Trp	0.093 ^c	1.0	$\ll 1.0 \times 10^{-4}$	40 ^d	50
Tyr308Phe	0.093 ^c	>50	1.2×10^{-4}	85 ^d	>98
Tyr308Gly	0.093 ^c	>50	2.0×10^{-3}	84 ^d	>98
Tyr308Ser	0.093 ^c	>50	5.3×10^{-3}	100 ^d	>98

^a Referred to the scheme in Figure 4. ^b % occ_{exp}, nicotinamide occupancy estimated experimentally from the $\Delta\epsilon$ value of the peak at ~ 500 nm; % occ_{calc}, nicotinamide occupancy calculated from K_{in} values. ^c Value of the WT enzyme assumed for all FNR variants. ^d Values from ref 5. ^e Value implicit in constant calculation.

NADP⁺ nicotinamide moiety (Figure 2). This explains why, based on considerations of the bipartite binding model, the *Anabaena* FNR C-terminal mutants show enhanced binding of NADP⁺, and in the case of these FNR mutants, the increased affinity for the NMN portion of the coenzyme drives the binding of the whole dinucleotide and produces stronger interactions. Additionally, it is worth noting the decay in the long-wavelength band observed in the case of the Tyr303Trp variant (putatively due to the charge transfer character of the interaction between the indole group of Trp and the isoalloxazine ring of FAD) upon complex formation with both NADP⁺ and NAD⁺ (Figure 2). Thus, the NADP⁺ and NAD⁺ difference spectra of the *Anabaena* Tyr303Trp FNR complexes show that nucleotide binding causes the disruption of this interaction, probably by displacement of the Trp residue from the isoalloxazine ring environment. However, this effect has not been reported in CP450R, as the nicotinamide appears unable to displace the Trp residue (40).

K_d data can be fitted to a simple model to obtain separate binding constants for the 2'P-AMP ($K_{a,2P-AMP}$) and nicotinamide ($K_{a,NMN}$) moieties (Figure 4 and Table 5). In this model, shown in Figure 4, it is assumed that the displacement of the C-terminal residue and the nicotinamide binding constitute a concerted event. This is the simplest model to account for the observed events; a further complication of the mechanism in which the C-terminal residue can switch between two conformations, flipping in and out of the pocket, is ignored in the calculations. This movement would create an equilibrium between "in" and "out" conformations, being the "out" conformation the reactive species. A slow equilibration between "in" and "out" conformations would convert the C1 species (Figure 4) in a bottleneck. As the full reduction of the WT and mutated enzymes with NADPH is quite fast (Figure 3 and Table 4), it can be assumed that the flipping of the C-terminal residue, if existent, proceeds in a short time scale and it is not rate-limiting. A second simplification assumes that, in the case of NAD⁺, the binding is only driven by the NMN moiety, and the influence of the 2'P-AMP moiety is negligible. Previous data support this bipartite binding model (5, 10, 15, 26). Thus, the values of $K_{a,NMN}$ are directly derived from the K_d values obtained for NAD⁺, whereas the values of $K_{a,2P-AMP}$ are derived from the K_d values obtained for NADP⁺, on the following assumptions: (1) nicotinamide occupancy for the *Anabaena* WT FNR–NADP⁺ complex is 0; (2) nicotinamide oc-

cupancy for the pea WT FNR–NADP⁺ complex is 14%, as previously estimated (5); (3) $K_{a,2P-AMP}$ is similar to WT for all of the mutant enzymes.

The calculated equilibrium constants (Table 5) are consistent with the proposed scheme. Two binding equilibria compete when FNR and the coenzyme are mixed (15). When NADP⁺/H is used, the equilibrium is driven through C1 (Figure 4), whereas in the case of NAD⁺/H the formation of C1 is negligible (6). Nevertheless, if the NMN moiety can replace the C-terminal residue, it could provide a different binding mode forming species C3 (Figure 4). To explain the recognition of NADP⁺/H, a sequential equilibrium has to be postulated (15), with an apparent equilibrium constant, K_{in} (Table 5). A low K_{in} value indicates that the interaction between the isoalloxazine ring and the C-terminal residue is much stronger than the interaction between the isoalloxazine ring and the nicotinamide moiety of NAD(P)⁺/H (stabilization of form C1 in Figure 4), whereas a high K_{in} value indicates the opposite situation (stabilization of form C3 in Figure 4). In most cases, the values determined suggest a strong displacement of the equilibrium in one way or the other. Only for the *Anabaena* Tyr303Phe and Tyr303Trp variants and the pea WT and Tyr308Trp can a value of K_{in} be estimated, thus indicating that the stacking interaction of the aromatic residue with the isoalloxazine ring of FAD has a comparable energy to that of the nicotinamide–FAD interaction. The NMN occupancy values estimated from the K_{in} (Table 5) show a good agreement with the experimental values derived from the difference spectra reported in this work (Table 2) and those of ref 5. It is remarkable the low % occ_{exp} obtained for the interaction of NADP⁺ with the *Anabaena* Tyr303Trp variant, which correlates with our structural studies showing no occupancy of the C-terminal position by the coenzyme NMN portion (Figure 6).

Three-dimensional structures of the Tyr303Trp FNR and the Tyr303Ser *Anabaena* FNR variants in complex with NADP⁺ have been solved (Figure 6). Unexpectedly, both structures are largely different. The Tyr303Trp FNR variant exhibits a nonproductive complex, similar to that reported for the FNR–NADP⁺ complex obtained by cocrystallization (15), in which the 2'P-AMP and pyrophosphate portions of the NADP⁺ are perfectly bound. In addition, the NMN moiety is placed in a new pocket created near the FAD cofactor with the ribose being in a tight conformation. Besides, the nicotinamide ring presents its B-face to the *re*

face of the FAD. On the other hand, the Tyr303Ser FNR variant exhibits a productive complex in which the NADP⁺ shows an extended conformation, with the nicotinamide ring close to the isoalloxazine ring and in the correct orientation to allow hydride transfer. This complex is similar to that obtained for Tyr308Ser and Tyr308Trp pea FNR variants with NADP⁺ (10). The 3D structures of the Tyr303Trp FNR and the Tyr303Ser FNR variants in complex with NADP⁺ agree with the two final steps proposed in the mechanism of molecular recognition and complex reorganization to provide the adequate orientation for hydride transfer (15). Structural comparison of *Anabaena* FNR complexes with those of higher plant FNRs points to relevant differences between the cyanobacteria and higher plant mechanisms, while in higher plants (pea) the presence of a Trp at the C-terminal position allows, at least partially, the nicotinamide ring to occupy the hydride transfer position (10); that is not the case in cyanobacteria. Thus, data in Table 5 fully agree with the three-dimensional structures of the complexes between C-terminal FNR variants and NADP⁺ for *Anabaena* and pea enzymes so far reported, showing that the nicotinamide ring does not displace the Trp side chain in the case of the *Anabaena* FNR Tyr303Trp variant in the same extension than in the case of the corresponding pea variant (Figure 6). Such data also indicate that modulation of NADP⁺/H vs NAD⁺/H affinity is highly influenced by the strength of the C-terminus–FAD interaction and that subtle changes between plant and cyanobacterial structures are able to modify the energy of that interaction. Analysis of the three-dimensional structures of free Tyr303Ser and Tyr303Trp *Anabaena* FNR variants also shows clear differences between them. While the presence of a Trp instead a Tyr maintains the 3D arrangement of the FNR, and a similar stacking interaction between isoalloxazine ring and Trp is produced, deletion of the aromatic residue at the 303 position substantially perturbs the structural framework around the C-terminal end. Additionally, the presence of a bulky residue (Trp) prevents the existence of the highly conserved water (W1) molecule (Figure 5A), while in the Ser variant this water is conserved and two others are also present making an H-bond network from W1 to the OH–Ser303 group (Figure 5B). Despite the lack of this water molecule in the Trp variant, the kinetics of hydride transfer exhibited for this mutant FNR is still acceptable (Table 4), and therefore, the crucial role assigned to this highly conserved water in the mechanism should be revisited. Thus, from the structural analysis we can assess that the presence of an aromatic ring at the C-terminal positions seems to be relevant not only in the catalytic mechanism but also in stabilizing the structural framework in the C-terminal region of the FNR. Such data also indicate that modulation of NADP⁺/H vs NAD⁺/H affinity is highly influenced by the strength of the C-terminus–FAD interaction and that subtle changes between plant and cyanobacterial structures may be able to modify the energy of that interaction.

The data here presented also show a clear relationship between k_{obs} values obtained by fast kinetic studies and steady-state k_{cat} (Tables 3 and 4). First, the k_{obs} values obtained for the reactions of the Tyr303Ser variant with either NADPH or NADH prove that the low efficiency observed for this mutant enzyme under steady-state conditions is not due to a lack of catalytic ability but rather to the strength of

the complex formed at the NMN portion of the coenzyme after the initial encounter. Such strong interaction does not allow dissociation after hydride transfer, preventing another steady-state cycle. In the reactions with NADH, steady-state k_{cat} values closely approach k_{obs} values obtained by fast kinetic studies (Table 4). This indicates that, for the reactions of WT FNR, Tyr303Phe, and Tyr303Trp with NADH the reductive half-reaction (reduction of the enzyme by NADH) becomes rate-limiting. There is no correlation for the Tyr303Ser variant, where the oxidative half-reaction (oxidation of FNR_{rd} by DCPIP) is the limiting step. Thus, in the reaction with NADH, the flavin reduction seems to be related to the fast rate ($k_{\text{obs}1}$) and not with the slow rate ($k_{\text{obs}2}$), as is seen clearly in the absorbance changes at 340 nm. The reaction with NADPH may proceed in a similar way, and thus the fast rate may comprise part of the flavin reduction process and not only the formation of the [FNR_{ox}–NADPH] charge transfer complex. We are currently studying these issues (J. Tejero, J. R. Peregrina, A. Gutiérrez, N. S. Scrutton, C. Gómez-Moreno, and M. Medina, manuscript in preparation).

In conclusion, all of these observations taken together provide valuable evidence of the displacement of the C-terminal residue in the case of all of the pea FNR forms and also in the *Anabaena* FNR mutants where the C-terminal Tyr has been replaced. Since all of these enzymes are functional, it is tempting to suggest that the C-terminal Tyr plays a sensitive role by modulating nicotinamide affinity but is by no means essential for hydride transfer. In this context, the relevance of that contribution could be gauged by considering that related enzymes that lack the Tyr at the FAD stacking position display turnover rates that are considerably slower than FNR forms that harbor typical C-terminal and FAD conformations. Optimization for catalytic efficiency in the chloroplast and cyanobacterial reductases might be related to the demands of the photosynthetic process that requires a very fast electron flow to sustain CO₂ fixation rates, whereas in organisms growing by heterotrophic metabolism or anoxygenic photosynthesis, FNR is more likely involved in pathways that proceed at a much slower pace.

REFERENCES

1. Arakaki, A. K., Ceccarelli, E. A., and Carrillo, N. (1997) Plant-type ferredoxin-NADP⁺ reductases: a basal structural framework and a multiplicity of functions, *FASEB J.* 11, 133–140.
2. Carrillo, N., and Ceccarelli, E. A. (2003) Open questions in ferredoxin-NADP⁺ reductase catalytic mechanism, *Eur. J. Biochem.* 270, 1900–1915.
3. Medina, M., and Gómez-Moreno, C. (2004) Interaction of ferredoxin-NADP⁺ reductase with its substrates: optimal interaction for efficient electron transfer, *Photosynth. Res.* 79, 113–131.
4. Karplus, P. A., and Faber, H. R. (2004) Structural aspects of plant ferredoxin:NADP⁺ oxidoreductases, *Photosynth. Res.* 81, 303–315.
5. Piubelli, L., Aliverti, A., Arakaki, A. K., Carrillo, N., Ceccarelli, E. A., Karplus, P. A., and Zanetti, G. (2000) Competition between C-terminal tyrosine and nicotinamide modulates pyridine nucleotide affinity and specificity in plant ferredoxin-NADP(+) reductase, *J. Biol. Chem.* 275, 10472–10476.
6. Medina, M., Luquita, A., Tejero, J., Hermoso, J., Mayoral, T., Sanz-Aparicio, J., Grever, K., and Gómez-Moreno, C. (2001) Probing the determinants of coenzyme specificity in ferredoxin-NADP⁺ reductase by site-directed mutagenesis, *J. Biol. Chem.* 276, 11902–11912.

- Karplus, P. A., Daniels, M. J., and Herriott, J. R. (1991) Atomic structure of ferredoxin-NADP⁺ reductase: prototype for a structurally novel flavoenzyme family, *Science* 251, 60–66.
- Bruns, C. M., and Karplus, P. A. (1995) Refined crystal structure of spinach ferredoxin reductase at 1.7 Å resolution: oxidized, reduced and 2'-phospho-5'-AMP bound states, *J. Mol. Biol.* 247, 125–145 (doi: 10.1006/jmbi.1994.0127).
- Serre, L., Vellieux, F. M., Medina, M., Gómez-Moreno, C., Fontecilla-Camps, J. C., and Frey, M. (1996) X-ray structure of the ferredoxin:NADP⁺ reductase from the cyanobacterium *Anabaena* PCC 7119 at 1.8 Å resolution, and crystallographic studies of NADP⁺ binding at 2.25 Å resolution, *J. Mol. Biol.* 263, 20–39.
- Deng, Z., Aliverti, A., Zanetti, G., Arakaki, A. K., Ottado, J., Orellano, E. G., Calcaterra, N. B., Ceccarelli, E. A., Carrillo, N., and Karplus, P. A. (1999) A productive NADP⁺ binding mode of ferredoxin-NADP⁺ reductase revealed by protein engineering and crystallographic studies, *Nat. Struct. Biol.* 6, 847–853.
- Dorowski, A., Hofmann, A., Steegborn, C., Boicu, M., and Huber, R. (2001) Crystal structure of paprika ferredoxin-NADP⁺ reductase. Implications for the electron transfer pathway, *J. Biol. Chem.* 276, 9253–9263.
- Aliverti, A., Faber, R., Finnerty, C. M., Ferioli, C., Pandini, V., Negri, A., Karplus, P. A., and Zanetti, G. (2001) Biochemical and crystallographic characterization of ferredoxin-NADP(+) reductase from nonphotosynthetic tissues, *Biochemistry* 40, 14501–14508.
- Morales, R., Charon, M.-H., Kachalova, G., Serre, L., Medina, M., Gómez-Moreno, C., and Frey, M. (2000) A redox-dependent interaction between two electron-transfer partners involved in photosynthesis, *EMBO Rep.* 1, 271–276.
- Kurusu, G., Kusunoki, M., Katoh, E., Yamazaki, T., Teshima, K., Onda, Y., Kimata-Arigo, Y., and Hase, T. (2001) Structure of the electron transfer complex between ferredoxin and ferredoxin-NADP(+) reductase, *Nat. Struct. Biol.* 8, 117–121.
- Hermoso, J. A., Mayoral, T., Faro, M., Gómez-Moreno, C., Sanz-Aparicio, J., and Medina, M. (2002) Mechanism of coenzyme recognition and binding revealed by crystal structure analysis of ferredoxin-NADP⁺ reductase complexed with NADP⁺, *J. Mol. Biol.* 319, 1133–1142.
- Karplus, P. A., and Bruns, C. M. (1994) Structure–function relations for ferredoxin reductase, *J. Bioenerg. Biomembr.* 26, 89–99.
- Chen, Z., Lee, W. R., and Chang, S. H. (1991) Role of aspartic acid 38 in the cofactor specificity of *Drosophila* alcohol dehydrogenase, *Eur. J. Biochem.* 202, 263–267.
- Clermont, S., Corbier, C., Mely, Y., Gerard, D., Wonacott, A., and Branlant, G. (1993) Determinants of coenzyme specificity in glyceraldehyde-3-phosphate dehydrogenase: role of the acidic residue in the fingerprint region of the nucleotide binding fold, *Biochemistry* 32, 10178–10184.
- Marohnic, C. C., Bewley, M. C., and Barber, M. J. (2003) Engineering and characterization of a NADPH-utilizing cytochrome *b₅* reductase, *Biochemistry* 42, 11170–11182.
- Scrutton, N. S., Berry, A., and Perham, R. N. (1990) Redesign of the coenzyme specificity of a dehydrogenase by protein engineering, *Nature* 343, 38–43.
- Bocanegra, J. A., Scrutton, N. S., and Perham, R. N. (1993) Creation of an NADP-dependent pyruvate dehydrogenase multi-enzyme complex by protein engineering, *Biochemistry* 32, 2737–2740.
- Tejero, J., Martínez-Júlvez, M., Mayoral, T., Luquita, A., Sanz-Aparicio, J., Hermoso, J. A., Hurley, J. K., Tollin, G., Gómez-Moreno, C., and Medina, M. (2003) Involvement of the pyrophosphate and the 2'-phosphate binding regions of ferredoxin-NADP⁺ reductase in coenzyme specificity, *J. Biol. Chem.* 278, 49203–49214.
- Adak, S., Sharma, M., Meade, A. L., and Stuehr, D. J. (2002) A conserved flavin-shielding residue regulates NO synthase electron transfer and nicotinamide coenzyme specificity, *Proc. Natl. Acad. Sci. U.S.A.* 99, 13516–13521.
- Nogués, I., Tejero, J., Hurley, J. K., Paladini, D., Frago, S., Tollin, G., Mayhew, S. G., Gómez-Moreno, C., Ceccarelli, E. A., Carrillo, N., and Medina, M. (2004) Role of the C-terminal tyrosine of ferredoxin-nicotinamide adenine dinucleotide phosphate reductase in the electron transfer processes with its protein partners ferredoxin and flavodoxin, *Biochemistry* 43, 6127–6137.
- Döhr, O., Paine, M. J., Friedberg, T., Roberts, G. C., and Wolf, C. R. (2001) Engineering of a functional human NADH-dependent cytochrome P450 system, *Proc. Natl. Acad. Sci. U.S.A.* 98, 81–86.
- Elmore, C. L., and Porter, T. D. (2002) Modification of the nucleotide cofactor-binding site of cytochrome P-450 reductase to enhance turnover with NADH in vivo, *J. Biol. Chem.* 277, 48960–48964.
- Sancho, J., and Gomez-Moreno, C. (1991) Interaction of ferredoxin-NADP⁺ reductase from *Anabaena* with its substrates, *Arch. Biochem. Biophys.* 288, 231–238.
- Medina, M., Martínez-Júlvez, M., Hurley, J. K., Tollin, G., and Gómez-Moreno, C. (1998) Involvement of glutamic acid 301 in the catalytic mechanism of ferredoxin-NADP⁺ reductase from *Anabaena* PCC 7119, *Biochemistry* 37, 2715–2728.
- Mendes, P., and Kell, D. B. (1998) Non-linear optimization of biochemical pathways: applications to metabolic engineering and parameter estimation, *Bioinformatics* 14, 869–883.
- Collaborative Computational Project Number 4 (1994) The CCP4 Suite: Programs for Protein Crystallography, *Acta Crystallogr. D* 50, 760–763.
- Leslie, A. G. W. (1987) Profile fitting, in *Proceedings of the CCP4 Study Weekend* (Machin, J. R., and Papiz, M. Z., Eds.) pp 39–50, SERC Daresbury Laboratory, Warrington, U.K.
- Navaza, J. (1994) AMoRe: an automated package for molecular replacement, *Acta Crystallogr. A* 50, 157–163.
- Brunger, A. T., Adams, P. D., Clore, G. M., DeLano, W. L., Gros, P., Grosse-Kunstleve, R. W., Jiang, J. S., Kuszewski, J., Nilges, M., Pannu, N. S., Read, R. J., Rice, L. M., Simonson, T., and Warren, G. L. (1998) Crystallography & NMR system: A new software suite for macromolecular structure determination, *Acta Crystallogr. D* 54, 905–921.
- Jones, T. A., Zou, J. Y., Cowan, S. W., and Kjeldgaard, M. (1991) Improved methods for building protein models in electron density maps and the location of errors in these models, *Acta Crystallogr. A* 47, 110–119.
- Laskowski, R. A., MacArthur, M. W., Moss, D. S., and Thornton, J. M. (1993) PROCHECK: a program to check the stereochemical quality of protein structures, *J. Appl. Crystallogr.* 26, 283–291.
- Hooft, R. W. W., Vriend, G., Sander, C., and Abola, E. E. (1996) Errors in protein structures, *Nature* 381, 272.
- Kraulis, P. J. (1991) MOLSCRIPT: a program to produce both detailed and schematic plots of protein structures, *J. Appl. Crystallogr.* 24, 946–950.
- Merritt, E. A., and Bacon, D. J. (1997) Raster3D: Photorealistic Molecular Graphics, *Methods Enzymol.* 277, 505–524.
- Lostao, A., Gomez-Moreno, C., Mayhew, S. G., and Sancho, J. (1997) Differential stabilization of the three FMN redox forms by tyrosine 94 and tryptophan 57 in flavodoxin from *Anabaena* and its influence on the redox potentials, *Biochemistry* 36, 14334–14344.
- Hubbard, P. A., Shen, A. L., Paschke, R., Kasper, C. B., and Kim, J. J. (2001) NADPH-cytochrome P450 oxidoreductase. Structural basis for hydride and electron transfer, *J. Biol. Chem.* 276, 29163–29170.
- Batie, C. J., and Kamin, H. (1984) Electron transfer by ferredoxin: NADP⁺ reductase. Rapid-reaction evidence for participation of a ternary complex, *J. Biol. Chem.* 259, 11976–11985.
- Batie, C. J., and Kamin, H. (1986) Association of ferredoxin-NADP⁺ reductase with NADP(H) specificity and oxidation–reduction properties, *J. Biol. Chem.* 261, 11214–11223.
- Krakow, G., Ammeraal, R. N., and Vennesland, B. (1965) The stereospecificity of the Hill reaction with triphosphopyridine nucleotide, *J. Biol. Chem.* 240, 1820–1823.
- Calcaterra, N. B., Pico, G. A., Orellano, E. G., Ottado, J., Carrillo, N., and Ceccarelli, E. A. (1995) Contribution of the FAD binding site residue Tyr 308 to the stability of pea ferredoxin-NADP⁺ oxidoreductase, *Biochemistry* 34, 12842–12848.
- Gutierrez, A., Doehr, O., Paine, M., Wolf, C. R., Scrutton, N. S., and Roberts, G. C. (2000) Trp-676 facilitates nicotinamide coenzyme exchange in the reductive half-reaction of human cytochrome P450 reductase: properties of the soluble W676H and W676A mutant reductases, *Biochemistry* 39, 15990–15999.
- Gutierrez, A., Paine, M., Wolf, C. R., Scrutton, N. S., and Roberts, G. C. (2002) Relaxation kinetics of cytochrome P450 reductase: internal electron transfer is limited by conformational change and regulated by coenzyme binding, *Biochemistry* 41, 4626–4637.

47. Konas, D. W., Zhu, K., Sharma, M., Aulak, K. S., Brudvig, G. W., and Stuehr, D. J. (2004) The FAD-shielding residue Phe1395 regulates neuronal nitric oxide synthase catalysis by controlling NADP⁺ affinity and a conformational equilibrium within the flavoprotein domain, *J. Biol. Chem.* 279, 35412–35425.
48. Murataliev, M. B., Feyereisen, R., and Walker, F. A. (2004) Electron transfer by diflavin reductases, *Biochim. Biophys. Acta* 1698, 1–26.

BI051278C